# REEXAMINATION OF PROTON-INDUCED REACTIONS ON $^{\mathrm{nat}}$Mo AT 19–26 MeV AND STUDY OF TARGET YIELD OF RESULTANT RADIONUCLIDES

Arshiya A. Ahmed[†], A. Wrońska[‡], A. Magiera

M. Smoluchowski Institute of Physics, Jagiellonian University
Łojasiewicza 11, 30-348 Kraków, Poland

M. Bartyzel, J.W. Mietelski, R. Misiak, B. Wąs

H. Niewodniczański Institute of Nuclear Physics Polish Academy of Sciences
Radzikowskiego 152, 31-342 Kraków, Poland

*(Received September 9, 2019; accepted October 31, 2019)*

As an alternative to reactor-based $^{99}$Mo/$^{99m}$Tc generator technology, many research groups have suggested the direct production of $^{99m}$Tc on highly enriched $^{100}$Mo through accelerators. For proton-induced reaction, there is a large discrepancy in 9–26 MeV beam energy range in the data available for the production of radionuclides impurities. In this work, we studied target yield and the cross section for the production of long-lived radionuclides produced in the $^{\mathrm{nat}}$Mo target irradiated with a proton beam of energy degraded from 26 to 19 MeV in the target. This constitutes the first step, which is a commissioning of the setup and a check of the method at the beam energy where cross sections of interest are large. The step was necessary before proceeding with more demanding measurements at lower energies. Target yield was derived using the measured activity of produced radionuclides. Total cross sections for all isotopes produced from $^{\mathrm{nat}}$Mo$(p, x)$ reactions are presented and compared with the previously available data, showing good agreement.

DOI:10.5506/APhysPolB.50.1583

## 1. Introduction

About 80% of diagnostic imaging techniques in nuclear medicine involve technetium-99 at meta-stable state ($^{99m}$Tc) radioisotope. Around 2011, the failure of two major reactors involved in the production of $^{99}$Mo, which is the

[†] arshiya.anees.ahmed@doctoral.uj.edu.pl
[‡] aleksandra.wronska@uj.edu.pl

generator of $^{99m}$Tc, made the nuclear physics community realize the upcoming shortfall in the production of these isotopes [1]. Soon afterwards, new production paths were proposed in the literature [2–5], exploiting proton beam accelerated in cyclotrons: through $(p, 2n)$ reaction on highly enriched $^{100}$Mo. It is still possible to produce $^{99}$Mo and $^{99m}$Tc by proton-induced reaction on natural molybdenum ($^{\text{nat}}$Mo). Using natural target will be advantageous if activity of other radioisotopes is sufficiently small. Molybdenum is also used in accelerator applications as corrosion resistant and refractory metal, thus it is important to study proton-induced reaction cross section at the intermediate energy range. A quite substantial database is available for cross section of proton-induced reactions on both $^{\text{nat}}$Mo and enriched $^{100}$Mo [2, 3, 6–19], but there are large discrepancies between individual data sets. Besides, there is insufficient experimental data available for the impurities produced along with the $^{99}$Mo/$^{99m}$Tc [20]. In all the previously reported data the shape of the excitation curve is generally similar, but they differ in magnitude by a factor of 2. Hence, in the present work, we measured the production cross sections of $^{99}$Mo, $^{99m}$Tc (direct production) and other long-lived radioisotope impurities produced in proton-induced reaction on natural molybdenum by standard single-target activation technique at 19–26 MeV energy range. We also determined directly from our experimental data the integral target yield in this energy range for all the radioisotopes produced in $^{\text{nat}}$Mo which could be identified in the gamma spectrum. In [16], authors have provided the recommended cross-section data for gamma emitting diagnostic radioisotopes using previously published data and new experimental data which is helpful in validating the produced data.

## 2. Experiment

### *2.1. Beam, target and irradiation procedure*

The target used in the experiment was natural molybdenum with the following isotopic composition: $^{92}$Mo 14.64%, $^{94}$Mo 9.18%, $^{95}$Mo 15.87%, $^{96}$Mo 16.67%, $^{97}$Mo 9.58%, $^{98}$Mo 24.29%, and $^{100}$Mo 9.74% [21], in the form of a metallic disc (25 mm in diameter, 0.5 mm thick and 99.9% pure) purchased from Goodfellow Cambridge Limited, UK. The thickness of the target was verified by weighing the target on the micro-balance and measuring the target's surface.

The irradiation was done at an external beam line of AIC-144 cyclotron in the Institute of Nuclear Physics Polish Academy of Sciences, Kraków, Poland. It is an isochronous cyclotron which is capable of accelerating protons in the form of a collimated beam with energy of 60 MeV and intensity of 65 nA. Since the cyclotron produces mono-energetic protons and beam energy cannot be varied, we used 99% pure aluminum foils (11.7 mm thick)

as degraders. The average beam energy at the exit of the degrader was calculated using SRIM [22] and Geant4 simulation software [23], and was found to be 26 MeV and the value energy straggling was 0.16 MeV. The target was irradiated for 5 hours. After the end of bombardment (EOB), the target was left to cool down for 18 hours (cooling time $t_c = 18$ h).

Gamma-ray attenuation and the beam spread was studied using Geant4 simulations. Gamma attenuation within the target was about 0.5% (on average). The dimension of the proton beam was measured using a fluorescent sheet at the position of the Al degrader. The diameter of the beam was 5 mm. Then the degrader beam size was 2 cm in diameter and at the exit of the target, the beam was 2.3 cm which is less than the diameter of the target. Hence, the entire beam was incident on the target.

### *2.2. Radioactivity measurement*

The measurements of activity (gamma-ray counting) were done using an energy and efficiency calibrated HPGe detector. The energy and efficiency calibration of the detector was performed using a set of standard sources ($^{133}$Ba, $^{60}$Co, $^{152}$Eu, $^{22}$Na, and $^{137}$Cs) for the sample-detector distance of 52 cm. The detector efficiency $\epsilon$ was described as follows:

$$\ln(\epsilon) = \sum_{n=0}^{4} a_n (\ln E)^n \,, \tag{1}$$

where $E$ [keV] is the gamma energy and $a_n$ are fitted coefficients. The sample was measured at the same distance as used for efficiency calibration.

The first registered spectrum is shown in Fig. 1. The list of identified in this study radionuclides is presented in Table I. The data for half-lives, gamma-ray energies and intensities of transitions in radionuclides were adopted from the Nuclear Data Service, IAEA [24].

### *2.3. Interference process corrections and cross-section determination*

As is discussed in [14, 15, 17, 18], many radionuclides produce gamma lines of the same or nearly the same energy. For example, radioisomers $^{94}$Tc and $^{94m}$Tc decay produce 871.09 keV gamma quanta. The isotopes decaying to the same product also emit gamma of the same energy $^{94}$Tc –$^{94}$Nb, $^{95}$Tc –$^{95}$Nb, and $^{96}$Tc –$^{96}$Nb. The most complicated case in our analysis is the 140.51 keV spectral line ($^{90}$Nb, $^{99}$Mo, $^{99m}$Tc).

To determine the cross section of $^{99m}$Tc direct production, one needs to use an intense beam for a short irradiation time and a short cooling period. For accurate estimation, both irradiation and cooling time should be shorter than $\frac{1}{10}^{\text{th}}$ of the half-life of $^{99m}$Tc [15]. One can then use the

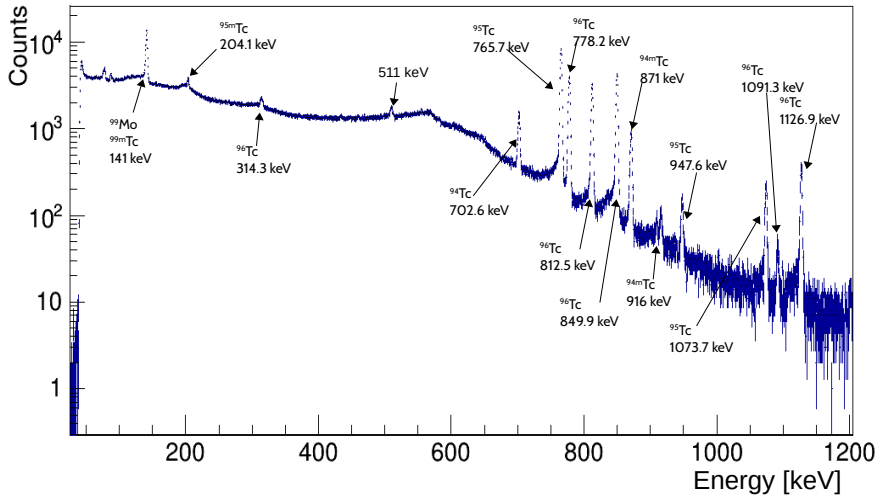


Fig. 1. Gamma spectrum of $^{\mathrm{nat}}$Mo target irradiated with a 26 MeV and 28.5 nA proton beam for five hours, recorded after 18 hours of cooling time.

standard activation formula (2) to find the direct production cross section of $^{99m}$Tc. If the above-mentioned conditions are not met, one needs to add appropriate corrections to the measured gamma yields or modify the standard activation formula [18]. In the calculations, we have neglected the contribution of $^{90}$Nb, since the $^{\mathrm{nat}}$Mo $(p,x)^{90}$Nb reaction cross section at 19–26 MeV is negligible [25]. Then the dependence of the activity for $^{99}$Mo is described by the standard activation formula (2) and for $^{99m}$Tc, the modified formula (3) is used

$$A(t) = n_0 I \sigma \left(1 - \mathrm{e}^{-\lambda t_{\mathrm{irr}}}\right) \mathrm{e}^{-\lambda t}, \tag{2}$$

$$\begin{aligned} A_{\mathrm{Tcm}}(t) = n_0 I \Bigg[ & \left(\sigma_{\mathrm{Tcm}} + P_{\mathrm{Mo}} \frac{\lambda_{\mathrm{Mo}}}{\lambda_{\mathrm{Mo}} - \lambda_{\mathrm{Tcm}}} \sigma_{\mathrm{Mo}}\right) \\ & \times \left(1 - \mathrm{e}^{-\lambda_{\mathrm{Tcm}} t_{\mathrm{irr}}}\right) \mathrm{e}^{-\lambda_{\mathrm{Tcm}} t} - P_{\mathrm{Mo}} \frac{\lambda_{\mathrm{Tcm}}}{\lambda_{\mathrm{Mo}} - \lambda_{\mathrm{Tcm}}} \\ & \times \sigma_{\mathrm{Mo}} \left(1 - \mathrm{e}^{-\lambda_{\mathrm{Mo}} t_{\mathrm{irr}}}\right) \mathrm{e}^{-\lambda_{\mathrm{Mo}} t} \Bigg], \end{aligned} \tag{3}$$

where subscripts Mo, Tcm refer to $^{99}$Mo and $^{99m}$Tc isotopes, $A$ is the activity of the isotope at time $t$, $\lambda$ is the decay constant, $I$ is beam current expressed as a number of incident particles per second, $n_0$ is the surface density of the target, $\sigma$ is reaction cross section. $P_{\mathrm{Mo}}$ is the decay fraction of $^{99}$Mo to $^{99m}$Tc which is 0.876, and $t_{\mathrm{irr}}$ refers to irradiation time.

TABLE I

Nuclear data for Tc and Mo radionuclides produced at 19–26 MeV proton on $^{nat}$Mo target. Gamma energies used in this study are in bold. Uncertainties of the half-life, gamma energies and the corresponding intensities in the last valid digits are in italics.

| Radionuclides | Half life ($T_{1/2}$) | | $E_\gamma$ [keV] | | $I_\gamma$ [%] | |
|---|---|---|---|---|---|---|
| $^{94}$Tc | 293 min | *1* | **702.622** | ***19*** | **99.6** | ***18*** |
| | | | 849.74 | *7* | 95.7 | *18* |
| | | | **871.091** | ***18*** | **99.9** | |
| $^{94m}$Tc | 52.0 min | *10* | **871.091** | ***18*** | **94** | |
| | | | 993.19 | *9* | 2.21 | *3* |
| | | | 1522.11 | *20* | 4.5 | *3* |
| | | | 1868.68 | *8* | 5.7 | *3* |
| $^{95}$Tc | 20.0 h | *1* | **765.794** | ***7*** | **93.82** | ***19*** |
| | | | 947.67 | *2* | 1.951 | *19* |
| | | | 1073.71 | *2* | 3.74 | *4* |
| $^{95m}$Tc | 61 d | *2* | **204.117** | ***2*** | **63.25** | ***13*** |
| | | | 582.082 | *3* | 29.96 | *5* |
| | | | 835.149 | *5* | 26.63 | *19* |
| $^{96}$Tc | 4.28 d | *7* | 314.337 | *71* | 2.43 | *24* |
| | | | **778.224** | ***15*** | **99.9** | |
| | | | **812.581** | ***15*** | **82** | ***4*** |
| | | | 849.929 | *13* | 98 | *4* |
| | | | **1126.965** | ***21*** | **15.2** | ***12*** |
| $^{99m}$Tc | 6.01 h | *1* | **140.511** | ***1*** | **89** | |
| $^{99}$Mo | 65.94 h | *1* | **140.511** | ***1*** | **89.43** | ***23*** |
| | | | 181.063 | *8* | 5.99 | *7* |
| | | | 739.50 | *2* | 12.13 | *12* |

As we can see from Eq. (3), activity of $^{99m}$Tc is the sum of two exponential components, one with decay constant of $^{99m}$Tc and the other of $^{99}$Mo, because during irradiation $^{99m}$Tc can be produced directly in the reaction $^{nat}$Mo$(p,x)^{99m}$Tc and through decay of $^{99}$Mo. To calculate the cross section for $^{99m}$Tc production deduced from the 140.51 keV photo peak, Eq. (3) is used and all other cross-section calculations are done using the standard activation formula.

### *2.4. Target yield (TY)*

For the known cross section, the target yield (TY) is calculated using Eq. (4), in which decay during the irradiation time is taken into account

$$\mathrm{TY}_{\sigma} = \frac{HN_{\mathrm{A}}\lambda}{Mze} \int_{E_{\min}}^{E_{\max}} \frac{\sigma(E)}{S(E)} \mathrm{d}E\,, \tag{4}$$

where $H$ is isotopic enrichment of the target, $N_{\mathrm{A}}$ is Avogadro's number, $M$ is atomic mass of the target, $z$ is atomic number of the incident particle, $e$ is electron charge, $S$ is the stopping power of the incident particle in the target, $E$ is the energy of the projectile, $E_{\max}$ is the maximum energy of the incident particle when it hits the target, and $E_{\min}$ is the minimum energy of the incident particle when it exits the target. Then, the saturation yield (SY) which specifies the activity at saturation is given by

$$\mathrm{SY}_{\sigma} = \frac{\mathrm{TY}_{\sigma}}{\lambda}\,, \tag{5}$$

and the target yield of measured activity of an isotope with activity $A$ at time $t_{\mathrm{c}}$ after the end of bombardment is

$$\mathrm{TY}_{\mathrm{exp}} = \frac{A\lambda \mathrm{e}^{\lambda t_{\mathrm{c}}}}{I(1-\mathrm{e}^{-\lambda t_{\mathrm{irr}}})}\,, \tag{6}$$

where $t_{\mathrm{c}}$ and $t_{\mathrm{irr}}$ are time of cooling and irradiation respectively. Experimental saturation yield ($\mathrm{SY}_{\mathrm{exp}}$) was determined using the value of $\mathrm{TY}_{\mathrm{exp}}$ calculated from Eq. (6) plugged into Eq. (5).

### *2.5. Estimation of uncertainties*

The uncertainties of the experimentally determined activity and cross-section data have their origin in uncertainties of the detection efficiency ($< 4\%$), the statistics of counting and photo-peak area determination ($< 3\%$), nuclear data and intensities of gamma lines used ($< 4\%$), and quality of the monitoring reaction data used in the evaluation ($< 7\%$) (discussed in Sec. 3.1 ), uncertainty in the beam energy leading to a change in monitoring reaction (5%) and foil thickness ($< 1\%$). The total uncertainty of measured cross section and yield was obtained by adding the above-mentioned uncertainties in quadrature. Obtained total uncertainties are 11% for cross section and 8% for yield.

## 3. Results and discussion

### *3.1. Absolute normalization to $^{nat}Mo(p,x)^{m+g96}Tc$ data*

The energy loss or degradation of the incident proton beam in the target was calculated using Geant4 [23] and SRIM [22] assuming incident proton energy as 26 MeV on $^{nat}$Mo. The target used in the experiment is quite thick, hence average of energies within the target defines energy scale of all deduced parameters. $^{nat}$Mo$(p,x)^{m+g96}$Tc monitoring reaction [26] was used to determine the integrated beam current. Gamma lines 778.22 keV, 812.54 keV and 849.86 keV were used in data evaluation. Integrated beam current obtained from this method was $28.5 \pm 3$ nA.

### *3.2. Cross section of Tc isotopes and $^{99}Mo$ production*

The determined production cross sections of $^{94}$Tc, $^{95}$Tc, $^{95m}$Tc, $^{96}$Tc, $^{99m}$Tc and $^{99}$Mo radionuclides are presented in Table II and compared with the existing data in Fig. 2. Since the target used in the experiment degraded the impinging beam energy by almost 7 MeV, the resulting calculated cross section is, in fact, averaged over the energy range of 19–26 MeV. Therefore, we compared our results with the existing data averaged over the same interval of proton energy. Figure 3 (a)–(f) shows the average cross-section comparison of our results with the literature data.

TABLE II

Measured cross section of $^{94}$Tc, $^{95}$Tc, $^{95m}$Tc, $^{96}$Tc, $^{99m}$Tc and $^{99}$Mo radionuclides produced in $^{nat}$Mo averaged over the proton energy range of 19–26 MeV.

| Radionuclides | Cross section [mb] |
|---|---|
| $^{94}$Tc | $60 \pm 7$ |
| $^{95}$Tc | $120 \pm 10$ |
| $^{95m}$Tc | $40 \pm 5$ |
| $^{96}$Tc | $120 \pm 10$ |
| $^{99m}$Tc | $110 \pm 10$ |
| $^{99}$Mo | $110 \pm 10$ |

To calculate the cross section of $^{94}$Tc, photo-peaks of 702.62 keV ($I_\gamma = 99.6\%$) and 871.09 keV ($I_\gamma = 99.9\%$) were used. $^{94m}$Tc also produces 871.09 keV ($I_\gamma = 94\%$) gamma line, but for the reasons discussed in Sec. 2.3, its contribution can be neglected. It is evident from Fig. 3 (a) that the obtained result is in agreement with the literature data, except those from Ref. [7].

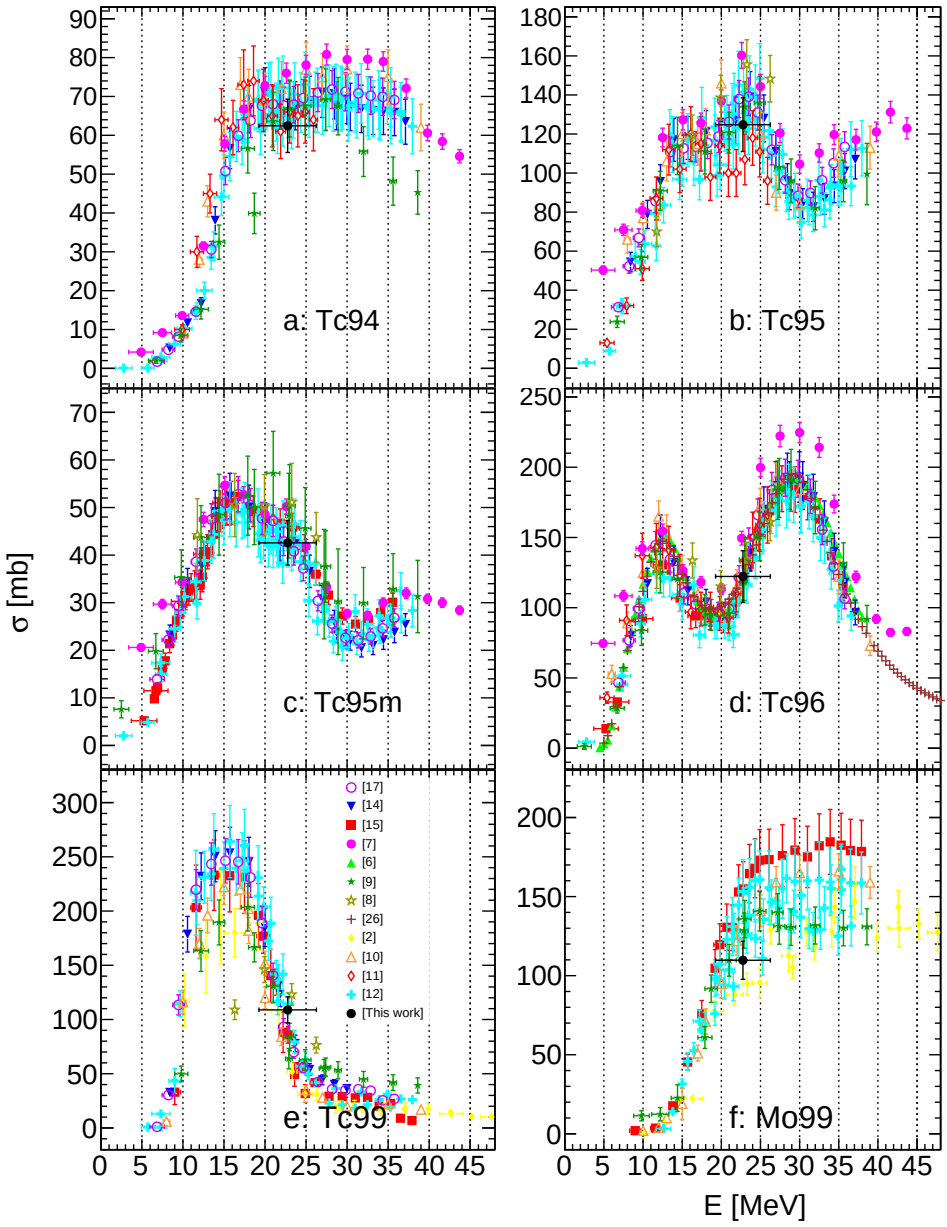


Fig. 2. Production cross section of radionuclide produced through $^{\mathrm{nat}/100}\mathrm{Mo}(p,x)$ reactions, where panels (a), (b), (c), (d), (e) and (f) represent cross sections of $^{94}$Tc, $^{95}$Tc, $^{95m}$Tc, $^{96}$Tc, $^{99m}$Tc and $^{99}$Mo, respectively. Here, the horizontal error bar represents the range of integration, not the energy uncertainty.

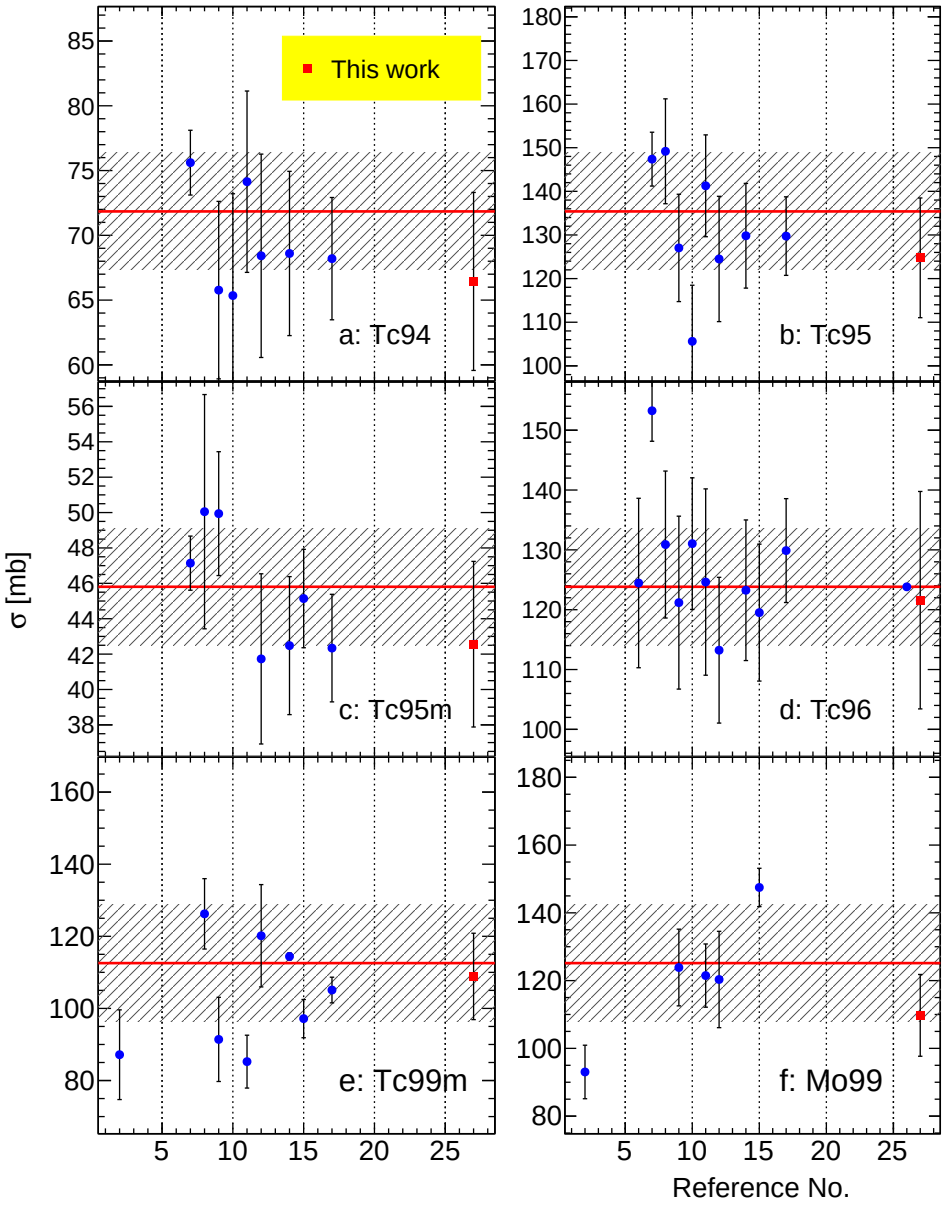


Fig. 3. Cross section of radionuclide produced through $^{nat/100}$Mo$(p, x)$ reactions averaged over the proton energy range of 19–26 MeV where panels (a), (b), (c), (d), (e) and (f), respectively, represent cross sections of $^{94}$Tc, $^{95}$Tc, $^{95m}$Tc, $^{96}$Tc, $^{99m}$Tc and $^{99}$Mo. The hatched bands represent standard deviation of literature data. The labels of $x$-axis represents the reference numbers from the reference list.

The production cross section of $^{95}$Tc is calculated by analyzing 765.79 keV ($I_\gamma = 93.82\%$) gamma peak and confirmed by the analysis of the 1073.71 keV ($I_\gamma = 3.74\%$) transition. Figure 3 (b) shows the present result for $^{95}$Tc radioisotope. Our result is consistent within the uncertainties with most of the data points, except for those from Refs. [10] and [11].

In order to calculate production cross section of $^{95m}$Tc radioisotope, we considered the 204.11 keV ($I_\gamma = 63.25\%$) gamma line. Possible interference of $^{95m}$Nb ($I_\gamma = 2.3\%$) gamma line with the same energy was insignificant for the detectors geometry used in the measurement. For the production of this radioisotope the obtained cross section agrees with the literature data (shown in Fig. 3 (c)).

$^{96m}$Tc ($T_{1/2}$ = 51 min) is a short-lived radioisomer of $^{96}$Tc ($T_{1/2}$ = 4.28 days). 98% of $^{96m}$Tc decays to $^{96}$Tc by the internal conversion process and emits very weak gamma spectral lines that are not suitable for quantitative study [8]. Although this isomer can also feed the 778.22 keV spectral line of $^{96}$Tc, its contribution can be neglected due to a large ratio of cooling time to its half-life. For the production cross section of $^{96}$Tc, we considered 778.22 keV ($I_\gamma = 99.9\%$) line and the results were cross-checked with 812.58 keV ($I_\gamma = 82.4\%$) transition, determined cross-section values from both photo-peaks were consistent. Figure 3 (d) shows the comparison of present data with other data available in the database. Our data is in good agreement with all other reported data except results from [7].

As discussed in Sec. 2.3, we used the 140.51 keV spectral line to calculate production cross section of $^{99m}$Tc and $^{99}$Mo. Reported cross sections are not cumulative. They were calculated separately for $^{99}$Mo and $^{99m}$Tc after suitable correction in the activation formula. For determination of $^{99}$Mo production cross section, we used data collected after at least 77 hours of cooling time, which justifies the neglect of contribution from directly produced $^{99m}$Tc. Average cross section of $^{100}$Mo$(p, x)^{99m}$Tc compared with other existing data is shown in Fig. 3 (e). Within the error bars, our result is in good agreement with other data points except those from Ref. [11], which are slightly lower. Figure 3 (f) shows the averaged cross-section comparison of $^{100}$Mo $(p, x)^{99}$Mo, our result is consistent with other data points within the error limits, only the data point from Ref. [15] deviates upwards from the trend.

### *3.3. Target yield and saturation yield*

Directly determined integral target yields of all studied radionuclides are presented in Table III. Integral target yield was calculated using Eq. (6). Target yield is expressed in MBq/$\mu$Ah (*i.e.* for 1 hour of irradiation at 1 $\mu$A beam current). The obtained results are shown in Fig. 4 as a function of

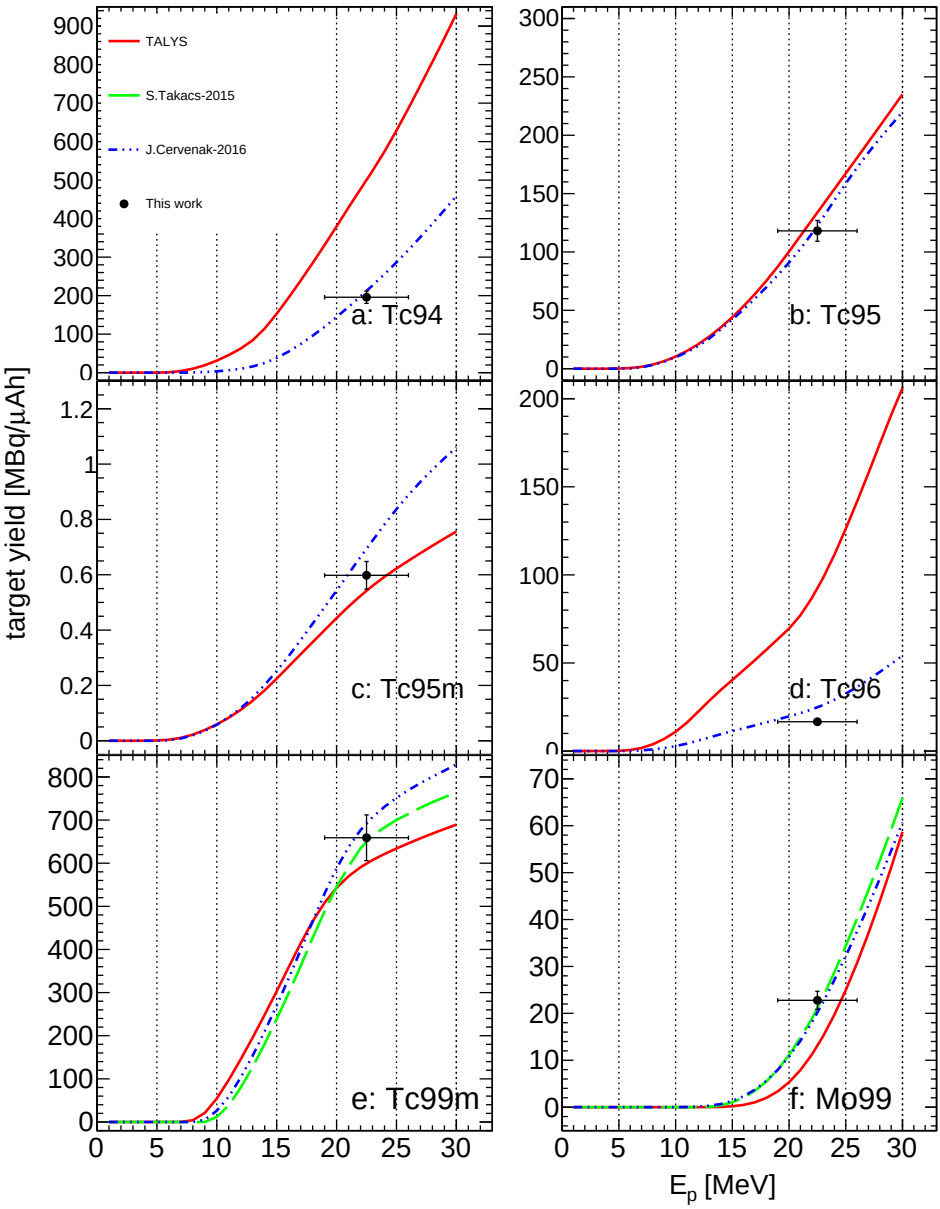


Fig. 4. (Color online) Integral TY of $^{nat}$Mo$(p, x)$ reaction; here, long dashed/green and dash-dotted/blue curves represent the experimental TY from [15] and [17], respectively, and the solid/red curve is from TALYS. Here, the error bar represents the range of integration not the energy uncertainties.

TABLE III

TY and SY of $^{94}$Tc, $^{95}$Tc, $^{95m}$Tc, $^{96}$Tc, $^{99m}$Tc and $^{99}$Mo radionuclides produced by proton irradiation on $^{nat}$Mo target.

| Isotope | TY [MBq/$\mu$Ah] | SY [MBq/$\mu$A] |
|---|---|---|
| $^{94}$Tc | 200 ± 20 | 1380 ± 110 |
| $^{95}$Tc | 120 ± 10 | 3410 ± 270 |
| $^{95m}$Tc | 0.60 ± 0.05 | 1290 ± 100 |
| $^{96}$Tc | 20 ± 1 | 2560 ± 200 |
| $^{99m}$Tc | 660 ± 50 | 5710 ± 460 |
| $^{99}$Mo | 20 ± 1 | 2190 ± 170 |

incident proton energy and are compared with TY from [17] and TALYS [27] predictions. In the case of $^{99}$Mo and $^{99m}$Tc, we have compared the results also with data from Ref. [15]. TY from [15] and [17] were calculated using the fitted experimental data (cross-section data was used from [28]) and stopping power of protons in molybdenum in the measured energy range. Similarly, TY from TALYS was calculated using cross-section data from TALYS.

As seen in Fig. 4, integral TY data is in good agreement with [17] and [15] within the error limits. In the case of $^{nat}$Mo$(p,x)^{94,96}$Tc, TALYS predictions are higher than the experimental data, in other cases, TALYS predictions are in agreement with experimental TY.

## 4. Conclusions

We measured the average cross section for the production of $^{94}$Tc, $^{95}$Tc, $^{95m}$Tc, $^{96}$Tc, $^{99m}$Tc and $^{99}$Mo radionuclides through $^{nat}$Mo$(p,x)$ reactions in the proton energy range of 19–26 MeV. The determined cross sections have been compared to existing data and they show consistency with most of them. The target yields were deduced from the measured activity of all listed radioisotopes. Target yields determined in the experiment have been confronted with the results of [15, 17, 27]. TALYS target yield predictions are found to be not in agreement with this experimental values in the case of $^{nat}$Mo$(p,x)^{94,96}$Tc.

Currently, the price of enriched Mo is about $30,000 per gram, whereas for $^{nat}$Mo the price varies from $0.25 to $0.80 per gram [29]. By using natural molybdenum targets, one can reduce the cost and meet the desired yield by increasing the irradiation time. Using protons of energies of 9–26 MeV will help to reduce the production of impurities. It was demonstrated that use of $^{nat}$Mo target could provide a very pure $^{99}$Mo source for extraction of $^{99m}$Tc with standard methods [7, 30].

As our results agree with other available data, the presented experiment and its results prove that the experimental setup is well-understood, with this data analysis procedure we will go for a measurements at lower energy, with stack-foil activation method.

This work was supported by the DSC 2017 grant intended to finance the development of young researchers and Ph.D. students of the Faculty of Physics, Astronomy and Applied Computer Science with the decision number MNSW: 7150/E-338/M/2017. The authors are thankful to the staff of AIC-144 cyclotron for the excellent work.

## REFERENCES

[1] T.J. Ruth, *La Physique AU Canada* **66**, 15 (2010).
[2] B. Scholten *et al.*, *Appl. Radiat. Isot.* **51**, 69 (1999).
[3] M.C. Lagunas-Solar *et al.*, *Int. J. Radiat. Appl. Instrum. A* **42**, 643 (1991).
[4] National Research Council, *Medical Isotope Production Without Highly Enriched Uranium*, The National Academies Press, Washington, DC, 2009.
[5] S. Takács *et al.*, *J. Radioanal. Nucl. Chem.* **257**, 195 (2003).
[6] S. Takács, F. Tárkányi, M. Sonck, A. Hermanne, *Nucl. Instrum. Methods Phys. Res. B* **198**, 183 (2002).
[7] M. Bonardi, C. Birattari, F. Groppi, E. Sabbioni, *Appl. Radiat. Isot.* **57**, 617 (2002).
[8] M.U. Khandaker *et al.*, *J. Korean Phys. Soc.* **48**, 821 (2006).
[9] M.U. Khandaker *et al.*, *Nucl. Instrum. Methods Phys. Res. B* **262**, 171 (2007).
[10] A.A. Alharbi, J. Alzahrani, A. Azzam, *Radiochim. Acta* **99**, 763 (2011).
[11] A.A. Alharbi *et al.*, *Medical Radioisotopes Production: A Comprehensive Cross-section Study for the Production of Mo and Tc Radioisotopes via Proton Induced Nuclear Reactions on $^{nat}$Mo*, in: *Radioisotopes — Applications in Bio-Medical Science*, Prof. N. Singh (Ed.), pages 3–26, 2011.
[12] F. Tárkányi *et al.*, *Nucl. Instrum. Methods Phys. Res. B* **280**, 45 (2012).
[13] P. Chodash *et al.*, *Appl. Radiat. Isot.* **69**, 1447 (2011).
[14] O. Lebeda, M. Pruszyński, *Appl. Radiat. Isot.* **68**, 2355 (2010).
[15] S. Takács *et al.*, *Nucl. Instrum. Methods Phys. Res. B* **347**, 26 (2015).
[16] F. Tárkányi *et al.*, *J. Radioanal. Nucl. Chem.* **319**, 487 (2019).
[17] J. Červenák, O. Lebeda, *Nucl. Instrum. Methods Phys. Res. B* **380**, 32 (2016).
[18] S.M. Qaim *et al.*, *Appl. Radiat. Isot.* **85**, 101 (2014).
[19] K. Szkliniarz *et al.*, *Mod. Phys. Lett. A* **32**, 1740012 (2017).
[20] S.M. Qaim, *Nucl. Med. Biol.* **44**, 31 (2017).

[21] J. Meija *et al.*, *Pure Appl. Chem.* **88**, 293 (2016).
[22] J.F. Ziegler, J.P. Biersack, M.D. Ziegler, SRIM code, version 2013.
[23] Geant4 (simulation software), version 10.2.3, 2017.
[24] Nuclear structure and decay data.
[25] M.S. Uddin *et al.*, *Appl. Radiat. Isot.* **60**, 911 (2004).
[26] A. Hermanne *et al.*, *Nuclear Data Sheets* **148**, 338 (2018).
[27] TALYS (software), version 1.9, 2018.
[28] Experimental Nuclear Reaction Data (EXFOR), 2018, database version of November 29, 2018.
[29] T. Michael Martin *et al.*, *J. Radioanal. Nucl. Chem.* **314**, 1051 (2017).
[30] M. Gumiela, J. Dudek, A. Bilewicz, *J. Radioanal. Nucl. Chem.* **310**, 1061 (2016).